Data-Driven Joint Demodulation and Decoding in THz Communication Systems

Abigail O. Oyekola[†], Imtiaz Ahmed[†], Danda B. Rawat[†], Ramesh Annavajjala^{††}, and Sachin Shetty^{†††}

[†]Howard University, Washington DC, USA

^{††}University of Massachusetts Boston, MA, USA

^{†††}Old Dominion University, Norfolk, VA, USA

Emails: abigail.oyekola@bison.howard.edu, imtiaz.ahmed@howard.edu, danda.rawat@howard.edu, ramesh.annavajjala@umb.edu, and sshetty @odu.edu

Abstract—This paper explores the impact of impairments such as phase noise (PN), additive white gaussian noise (AWGN), and in-phase and quadrature (IQ) imbalance distortions in corrupting transmitted signals across a point-to-point terahertz (THz) communication system. Deep learning (DL) is leveraged at the receiver end to develop a deep neural network (DNN) based multi-label classification (MLC) t hat p erforms t he f unctions of denoising, demodulating, and decoding (DeNMC) in a single operational block. Datasets for the DL assisted DeNMC were trained offline over a wide range of signal-to-noise ratios (SNRs) and deployed online for real-time data processing at the receiver. In this paper, we show that artificial i ntelligence (AI) can help mitigate the PN effect and IQ imbalances. Simulation results proved that implementing DL assisted DeNMC yields better performance than the conventional non-AI receiver while achieving lower computational complexity.

Index Terms—THz bands, phase noise, IQ imbalance, deep learning, joint denoising, demodulation, and decoding.

I. INTRODUCTION

The surge in research explores integrating Artificial Intelligence (AI) into the terahertz (THz) wireless communication physical layer. Governed by defined signal processing, modulation, and error correction, the THz spectrum, situated between microwave and infrared frequencies, promises higher bandwidth [1]. Unique challenges such as atmospheric absorption and path loss arise. AI adapts to this complexity, optimizing THz communication systems by mitigating challenges and enhancing overall performance.

A. Convergence of AI and THz Technology

The convergence of AI and THz technology redefines wireless communication capabilities. Machine Learning (ML), in particular, Deep Learning (DL) based algorithms, adapt to dynamic channel conditions, impairments, and interference, impacting network quality. The integration of AI with transmission and reception capability enables novel applications in wireless imaging, spectroscopy, medical diagnostics, healthcare, aerospace, medical technology, security, defense, entertainment, and material science. Growing interest in AI for the physical layer of THz wire-less communication is fueled by several factors. Leveraging THz's higher bandwidth, AI dynamically adapts modulation

This work is supported in part by the DoD Center of Excellence in AI/ML (CoE-AIML) at Howard University under Contract W911NF-20-2-0277

schemes, optimizing beamforming for stronger and focused signal transmissions. Accurate channel estimation, equalization, and signal distortion compensation counter multipath effects and path loss, enhancing overall signal quality.

Conventional block-based designs in THz-band communication lack guaranteed overall optimal performance [2]. This gap leads to the adoption of AI tools, optimizing error rate and throughput while managing operational and computational complexity in THz wireless communication networks. In the physical layer, AI supplements conventional designs with advanced algorithms, surpassing the traditional approach and addressing impairment complexities for optimized THz signal quality.

B. Integration of AI Tools in THz Wireless Communication

The rising demand for high-speed data necessitates exceptional throughput. AI optimizes resource allocation, modulation schemes, and signal processing for efficient communication network performance, adapting to interference levels and minimizing error rates. It reduces manual interventions, adapts to evolving demands, and mitigates phase noise (PN) effects in THz frequencies through random phase variation estimation and compensation, enhancing signal quality alongside correcting in-phase and quadrature-phase (IQ) imbalances for improved system performance.

Adopting AI in channel equalization, adaptive demodulation, and dynamic decoding remarkably improves signal recovery, minimizes error rates, and optimizes data rates compared to conventional schemes [3]–[7]. Researchers leverage AI to enhance link reliability and throughput, minimize BER, and compensate for PN and IQ Imbalance, optimizing Quality of Service (QoS) [16]–[19]. AI-based approaches like fully connected Deep Neural Networks (DNNs), Recurrent Neural Networks (RNNs), Convolutional Neural Networks (CNNs), and denoising autoencoder eliminate conventional signal processing blocks [2], [8]–[15].

C. Linear Block Codes

DNN-based channel decoder designs for linear block codes, including Hamming codes, BCH codes, and Reed-Solomon codes, show promise for enhancing error correction in communication systems [3]–[5], [14]. Offline-trained fully connected

DNN decoders, integrated online in THz transmission, improve error correction performance for codes like (7,4) Hamming Code (HC) [14]. Techniques in [3]–[5] optimize decoding processes and enhance Bit Interleaved Coded Modulation (BICM) receivers for LDPC-coded DCO-OFDM networks, predicting and optimizing probabilities for Log Likelihood Ratio (LLR) detectors.

D. Main Contributions of This Work

In this paper, we introduce joint denoising, demodulating, and decoding (DeNMC) functional block, a THz receiver employing multi-label classification (MLC), and a binary class approach via a fully connected DNN [20]–[24]. Our focus is to evaluate its bit error rate (BER) performance under varying signal-to-noise ratios (SNRs) in the presence of PN and IQ imbalance during THz communication. DNN training involves diverse SNR scenarios. Comparative analysis with non-AI approaches is conducted, encompassing PN and IQ imbalance compensations. The paper is organized with an introduction (Section I) and system model (Section II), followed by an elaborate discussion on DL-assisted DeNMC (Section III). Simulation results and discussion are presented in Section IV, whilst Sections V and VI covers the conclusion and references, respectively.

II. SYSTEM MODEL

In the point-to-point (P2P) THz wireless communication system considered for this study (see Fig. 1), the transmitted signals is encoded using the $(e^{'},f^{'})$ channel coding. In the channel encoding of $\tilde{e}=\beta\tilde{e}$ and $\tilde{f}=\beta\tilde{f}$, integral β is the number of bits that represents an information for a given channel coding scheme. For instance, we set $\beta=1$ for binary Hamming code. The encoded message a containing f bits of information are then transmitted to the modulator section of the communication channel.

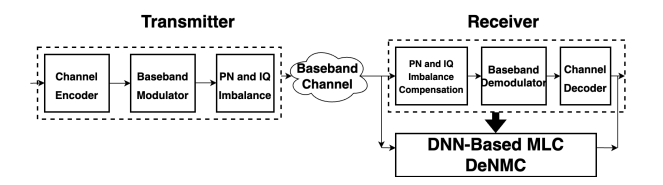


Fig. 1. P2P THz Communication link with Conventional vs. DNN-Based AI Receiver Processing.

The encoded bits are modulated using the baseband modulation scheme (e.g., Binary Phase-Shift Keying (BPSK), Quadrature Phase Shift Keying (QPSK), etc.). The modulated signal is then corrupted with the THz-band specific impairments, PN and IQ Imbalance before passing it through the Additive White Gaussian Noise (AWGN) to imitate a real-life scenario of a corrupted THz band signal. The impaired modulated THz signal is transmitted to the receiver over the baseband channel, assuming that the transmitter and receiver are in perfect synchronization.

At the receiver end of the DNN-based THz communication network, the weight of the input and output training symbols for any given epoch p is 2e for the $(e^{'},f^{'})$ linear block code modulation scheme, where $e=e^{'}$ given $e=\log_2(e^{'}+1)e^{'}$ and $f=f^{'}$ given that $f=\log_2(f^{'}+1)f^{'}$.

At any given time interval i, the discrete-time baseband THz wireless communication model is expressed as:

 $y[i] = b[i] + c[i] + d[i], i \in \{1, 2, 3, \cdots, I\}$ (1) where y[i] represents the complex (real and imaginary) signal at the receiver, b[i] is the transmitted signal after modulation from the baseband modulator module, c[i] is composed of the THz noisy impairments, and d[i] denotes the AWGN at zero mean (μ) and variance (σ^2) . In this paper, we defined the SNR derived from the received signal as $\gamma = M_b/\sigma^2$, where M_b refers to the energy of the received signal.

III. DL ASSISTED MLC DENMC ARCHITECTURE

DNN-based channel decoding entails training a deep neural network to replace traditional decoding algorithms. The neural network learns to map received noisy codewords to the most likely transmitted ones, enhancing error correction. Training involves pairs of clean and noisy codewords, with clean codewords as DNN inputs and noisy codewords as target outputs.

To train the DNN in a supervised learning approach utilizing the MLC technique, each input is mapped with a number of target labels simultaneously to represent the number of nodes in a binary indicator array (of 0's or 1's) at the DNN output layer [21].

A. Generation of Training Dataset

We represent \mathcal{P} as the training counts of epochs and \mathcal{Q} as the counts of batches for each epoch. \mathcal{Q} denotes the all training symbols employed for training in the given epoch. For a given $p \in \{1, 2, 3, ..., P\}$, the transmitter generates \mathcal{A}_p sets of message data bits to train the DL Assisted MLC DeNMC. These \mathcal{A}_p were mapped to the channel encoded data bit sequence λ_p before passing the encoded λ_p to the baseband modulator module to derive the modulated data symbols \mathcal{B}_p , $p \in \{1, 2, 3, ..., P\}$. The modulated data symbols \mathcal{B}_p was then contaminated with THz impairments of PN, IQ Imbalance distortions, and complex-valued AWGN to obtain the received sequences \mathcal{F}_p , $p \in \{1, 2, 3, ..., P\}$. Finally, the input and output training sequence was established as $\{\mathcal{F}_1, \mathcal{F}_2, \mathcal{F}_3, ..., \mathcal{F}_p\}$ and $\{\mathcal{A}_1, \mathcal{A}_2, \mathcal{A}_3, ..., \mathcal{A}_p\}$ respectively.

In this study, the real and imaginary parts of complex variable F was represented by $\Re\{y\}$ and $\Im\{y\}$ such that $F_p, p \in \{1,2,3,\cdots,P\}$ is expressed as $[\Re\{y_{1p}\},\Re\{y_{2p}\},\cdots,\Re\{y_{np}\},\Im\{y_{1p}\},\Im\{y_{2p}\},\cdots,\Im\{y_{np}\}]^T$. Furthermore, $A_p, p \in \{1,2,3,\cdots,P\}$ was denoted as $[a_{1p},a_{2p},a_{3p},\cdots,a_{f\log_2(H)p}]^T$. We represented the samples of the transmit information bit and the received symbols with d_{tp} and y_{tp} such that $p \in \{1,2,3,\cdots,P\}$ and $t \in \{1,2,3,\cdots,n\}$ respectively.

The complex valued y_{tp} was decomposed into the real and imaginary parts, therefore the size of input training symbols F_p , $p \in \{1, 2, 3, \dots, P\}$ is 2e. In the (7,4) Hamming code BPSK modulation scheme, the \mathcal{A}_p and F_p consisted of 4 bits

and 14 symbols respectively. More so, F_p and A_p consisted of 2e worth of data symbols and $f \log_2 H$ worth of data bits respectively. A fully connected DNN with 2e input nodes and $f \log_2(H)$ output labels was developed and trained with input and output training sequences to model the MLC DL assisted (DNN based) DeNMC.

B. Model Parameter Optimization

The parameters for the MLC DL assisted (DNN based) module was defined as \beth_l $\{\partial_{1l}, \partial_{2l}, \cdots, \partial_{Nl}, \theta_{1l}, \theta_{2l}, \cdots, \theta_{Nl}\}$ for a given hiddenlayer $l \in \{1, 2, 3, \dots, \mathcal{L}\}$. θ and ∂ signifies the bias factors and weight respectively. Similarly, \mathcal{L} indicates the aggregate amount of hidden layers, while \mathcal{N} symbolizes the aggregate amount of neurons in hidden-layer h. In training the MLC DL assisted (DNN based) DeNMC, A_p and F_p datasets was employed whilst optimizing $\beth = \{ \beth_1, \beth_2, \beth_3, \cdots, \beth_{\mathcal{L}} \}$ using:

$$\beth^* = \arg\min \mathcal{E}(\mathcal{A}_p, \hat{\mathcal{A}}_p) \tag{2}$$

The MLC DL assisted (DNN based) DeNMC output known with the estimation of A_p was marked as A_p , whilst the binary cross-entropy loss function was designated as \mathcal{E} for each label [23]. This binary cross-entropy loss function penalizes the model for predicting the wrong presence/absence of each label. Employing the softmax activation function at the MLC output layer, stochastic gradient decent approach and the back propagation algorithms (e.g., stochastic gradient descent (SGD), Adam, RMSprop, etc.) was utilized for the optimization of the DL assisted (DNN based) MLC as suggested by [20]. The softmax activation function convert a vector of raw scores or logits into a probability distribution over multiple classes by ensuring that the output values are in the range [0,1] and that they sum up to 1, making it suitable for modeling probabilities for multiple classes. More so, the cross-entropy loss measures the dissimilarity between the predicted probabilities and the true labels, and thereafter updates the model's weights through backpropagation..

C. DeNMC Model

As earlier stated, the MLC DL assisted (DNN based) DeNMC is trained and deployed online for joint demodulating and decoding of received signal, and making predictions at the receiver end of the THz wireless communication network. The signals $\{y[i], y[i+1], y[i+2], \cdots, y[i+n-1]\}$ received by the THz receiver are inputted into the MLC DL assisted (DNN based) DeNMC that outputs $\{\hat{a}_1, \hat{a}_2, \hat{a}_3, \cdots, \hat{a}_{f \log_2(H)}\}$. The decoded bit for the transmitted data bit a_c is regarded as \hat{a}_c , such that $c \in \{1, 2, 3, \dots, f \log_2(H)\}.$

IV. SIMULATION RESULTS

A. IQ Imbalance

The IQ imbalance was designed by applying gain imbalance (with different factors for the I and Q components) and phase imbalance to the complex-valued \mathcal{D} signal can be represented as follows:

$$\mathcal{I}\mathcal{Q}_{imb} = A(\alpha_{\mathcal{I}}\mathcal{D}_{\mathfrak{Re}} + i\alpha_{\mathcal{Q}}\mathcal{D}_{\mathfrak{Im}})e^{j\theta}$$
 (3)

Here, \mathcal{D} represents the data symbols, the loop filter coefficient (α) was set to 0.5, and we employed A = 1. A phase imbalance angle (radians) of $\theta = 0.5$ was used to introduce phase imbalance. A gain imbalance factor for the I (in-phase) and Q (quadrature) components were assigned to $\alpha_{\mathcal{I}}=8$ and $\alpha_{\mathcal{Q}}=5$ respectively. From the complex-valued signal \mathcal{D} containing the data symbols with the added phase noise, we extracted its real part and imaginary parts as $\mathcal{D}_{\mathfrak{Re}}$ and $\mathcal{D}_{\mathfrak{Im}}$ respectively. To introduce the gain imbalance, we calculated the weighted combination of the real and imaginary parts using $\vartheta_{\mathcal{I}}\mathcal{D}_{\mathfrak{Re}} + i\vartheta_{\mathcal{Q}}\mathcal{D}_{\mathfrak{Im}}$. To simulate the phase imbalance, a phase shift of $e^{j\theta}$ was introduced to the THz signal. Thereafter, the combination of the gain and phase imbalance was scaled by A and stored in the variable IQImb to simulate the effects of IO Imbalances on the received THz signal.

B. Phase Noise

```
Algorithm 1: Baseline Algorithm
```

```
Input: "Pilot and Data" signals: T_x(PDs)
Output: Transmission Signal: TxSig
Assign phase noise variance: \sigma^2 = V(t_x)
Initial Phase noise for THz RF impairments: \theta_{t_x}
Implementing the Phase-Locked Loop (PLL)
 Algorithm
for Phase Noise Algorithm do
```

```
foreach PhaseNoiseGeneration in TxSiq do
    for \Theta(idx) in length(T_x(PDs)) do
        Generate a random value from a normal
          distribution with mean 0 and standard
          deviation: \delta\Theta(idx) = \sqrt{\vartheta_{t_x}} \cdot \text{randn}(1,1).
        Update the values of \theta_{t_x} based on the
          generated \delta\Theta(t_x) values.
    end
```

Modulates the $T_x(PDs)$ signal by applying a phase shift (i.e., a complex exponential term with a phase) to each element based on the values in the array $\Theta(t_x)$.

end

end

In Algorithm 1, we describe the PN generation process to be applied to the transmitted signal $T_x(PDs)$, varying it for different testing phases to emulate shifts in carrier frequency states. Applying $e^{j\theta}$ distorted $T_x(PDs)$ based on specified PN levels. The resulting signal, stored in T_xSig , includes Pilotand Data signals with added phase noise. At the THz receiver, the DL-assisted DeNMC jointly demodulates and decodes the received message bits in a single module (refer to Fig. 1). Post DeNMC, y[i] output feeds MLC DeNMC offline training, predicting accuracy for transmitted signal x[i] in extensive SNRs using a[i] output datasets.

C. BER Performance

The BER performances of the DL assisted DeNMC proposed in our study was appraised for jointly denoising, demodulating, and decoding the received THz signals, which was then assessed against our baseline technique revised. Although, our study can be utilized for any baseband modulation schemes and advanced linear block codes, we illustrated the results for BPSK and Quadrature Phase Shift Keying (QPSK) for the linear baseband modulation schemes, and (7,4) Hamming codes for the linear block channel coding schemes throughout the course of this study based on the below plots:

- 1) **Plot 1:** BPSK modulation and (7,4) Hamming code
- 2) Plot 2: QPSK modulation and (7,4) Hamming code

In the MATLAB-based traditional block-based framework, we initiated a simulation by generating 10^5 random data bits subjected to (7,4) Hamming coding and modulation, resulting in $7*10^5$ data points. Simulating THz signals, IQ imbalance was applied. An additional $7*10^4$ Pilot samples were generated, resulting in $77*10^4$ samples (totSamples). The totSamples dataset was segmented into 100 chunks of Pilot and Data samples each, thus dividing totPilotSamples and totDataSamples to 100 and 1000 data points respectively in each chunk. We then arranged pilotAndData (representing TxSig) into arrays of intertwined Pilot and Data samples using $\{Pilot, Data, Pilot, Data, Pilot, ..., Data\}$ array arrangement. The spliced TxSig underwent phase noise (PN) from Algorithm 1 and AWGN before transmission to the receiver node.

At the MATLAB receiver end, PN estimation occurred based on Pilot samples. Non-linear interpolation (Spline method) was applied to create a smooth curve. Extracting Data samples, we used estimated PN from Pilot time slots to predict PN in Data time slots. PN and IQ imbalance compensations were implemented on RxSig before proceeding with block-by-block demodulation and decoding for the traditional block-based approach. A BER analysis was conducted to evaluate the performance of the conventional non-AI DeNMC module and compare it with our proposed DNN approach.

For the proposed DNN approach, the simulation platform was designed in Python framework where the deep learning DeNMC THz wireless communication was simulated with Tensorflow/Keras modules [26]. 10^5 data bits and noise samples was generated for the DL assisted (DNN based) module training purpose, whilst another 10^5 random data bits and noise samples was created validating our simulation results. THz impurities of PN and IQ Imbalance parameters described in the section II, equation (3), and algorithm 1, alongside AWGN was implemented throughout the simulations to obtain BER for different PN states. It is worth noting that for our proposed deep learning based DeNMC approach, we bypassed PN and IQ imbalance compensations on RxSig before exporting data points to the Python environment for AI-enabled THz wireless communication assessments.

D. BPSK Baseband Comparison Between Performance of AI and non-AI Based Models

The BER performances of our proposed DL assisted DeNMC for BPSK baseband modulation was analyzed in Fig. 2 to encompass SNRdB range -15:2:15. The conventional BPSK baseband model simulated the $BER\ nonAI$

curve, while the DNN based BPSK baseband model simulated the $BER\ AI$ curve. Each layer of the neural network model consisted of two hidden layers and 20 neurons.

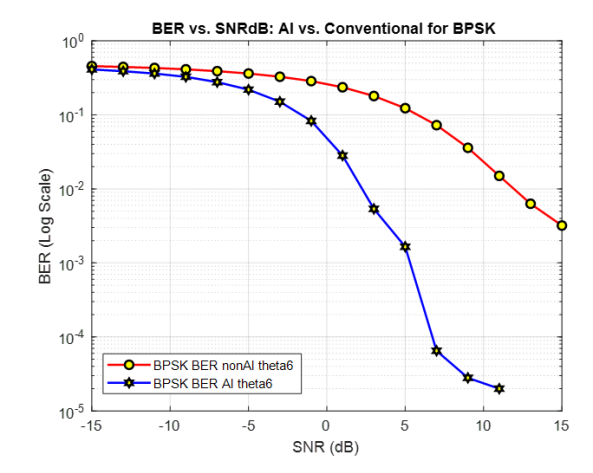


Fig. 2. BER vs SNRdB: AI-based vs. Conventional.

Between (-15:2:-10)dB, the improvement of the BER AI curve over the BER nonAI curve was not significantly noticeable. From (-10:2:-5)dB, we observed a slight improvement in our proposed DL assisted DeNMC for BPSK baseband modulation. Our major improvement was recorded from (1:2:15)dB, where we have the BER AI curve improving and optimizing our THz wireless communication by reducing the amount THz impairments effects on the THz signal when compared with the conventional block-based approach in the BER nonAI curve. The most substantial improvements were observed between (7:2:15)dB.

However, with an increase in SNR, the effects of phase noise, IQ imbalance, and other impurities in the THz wireless communication signal diminished, thus reducing the effectiveness of phase noise and IQ imbalance compensation, and even the artificially intelligent elimination of THz impairments in the signal. This is not to say that these proposed mediums of eliminating impairments in the signal are not effective, it just shows that the signal volume is sufficiently high enough to truncate the effects of impairments in the THz signals at higher SNR values. Nevertheless, both techniques (the DNN-based method or the conventional method with compensations) consistently provided enhanced performance compared to uncompensated scenarios, even at higher SNR levels.

Furthermore, we observed that whilst trying to drastically reduce the impacts of the THz impairments in the RxSig signals at mid and high SNR values of the considered range, the rate of BER reduction in the MLC DL assisted DeNMC was significantly impressive and outperformed the conventional method deployed with phase noise and IQ imbalance compensation. As seen in Fig. 4, as the PN increased, our model performed optimally to eliminate the effects of PN and IQ imbalance in the signal. Moreso, as the SNR ranges increases, the MLC DL assisted DeNMC (AI) demonstrated optimized BER outcomes which were quicker and more efficient than the

traditional model (non-AI). This shows the effectiveness and superiority of utilizing the proposed DeNMC to gain lower BER and optimal THz band signals than non-AI block-based signal processing schemes at the receiver end of the THz wireless communication network.

E. QPSK Performance Comparison Between AI and non-AI Based Models

The BER performances of our proposed DL assisted DeNMC for Quadrature Phase Shift Keying (QPSK) baseband modulation i.e., Plot 2 was assessed in Fig. 3 for SNRdB range (-15:15:2)dB. Similarly, the conventional QPSK baseband model simulated $BER\ nonAI$ curve, while the DNN based QPSK baseband model simulated $BER\ AI$ curve. Again, each layer of the neural network model consisted of two hidden layers and 20 neurons.

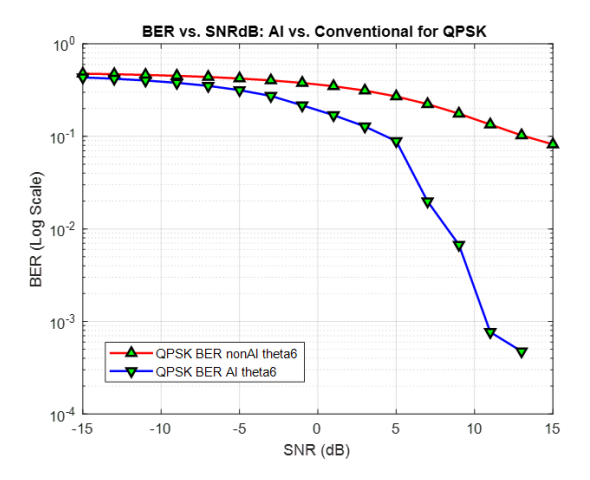


Fig. 3. BER vs SNRdB: AI-based vs. Conventional.

In the SNR range of -15dB to -5dB, the enhancement in the BER for Artificial Intelligence (AI) (i.e., the BER AI curve) was not notably discernible compared to the non-AI scenario (i.e., BER nonAI curve). However, within the SNR range of -5dB to -3dB, a marginal improvement was observed in the performance of our proposed Deep Learning (DL) assisted DeNMC for QPSK baseband modulation. The significant advancements in BER optimization were particularly pronounced in the range of 5dB to 15dB SNR, where the AI-enabled curve showcased superior performance. Notably, the most substantial improvements occurred in the SNR range of 11dB to 15dB. This highlights the efficacy of our DL approach in mitigating THz impairments and optimizing the THz wireless communication system, outperforming the conventional block-based approach represented by the QPSK non-AI curve.

However, with an increase in SNR, the effects of phase noise, IQ imbalance, and other impurities in the THz wireless communication signal diminished, thus reducing the effectiveness of phase noise and IQ imbalance compensation, and even the artificially intelligent elimination of THz impairments in the signal. The rate of BER reduction in the MLC DL assisted DeNMC was impressive and outperformed the conventional

method (deployed with phase noise and IQ imbalance compensation) at mid and high SNR values, as is evident in the rate of BER reduction between both methods of noise and THz impurities elimination.

Increasing PN to observe the effectiveness of our proposed model as seen in Fig. 4 where curves with *theta6* have a lower PN than curves with *theta10*, our model performed as expected at higher phase noise to eliminate the effects of PN and IQ imbalance in the signal. Moreso, as the SNR ranges increases, the MLC DL assisted DeNMC (AI) demonstrated optimized BER outcomes which were quicker and more efficient than the traditional model (non-AI). Evidently, our proposed DeNMC displayed lower BER than non-AI blockbased optimal signal processing schemes.

F. BPSK vs. QPSK Baseband Comparison Between Performance of AI and non-AI Enabled Models

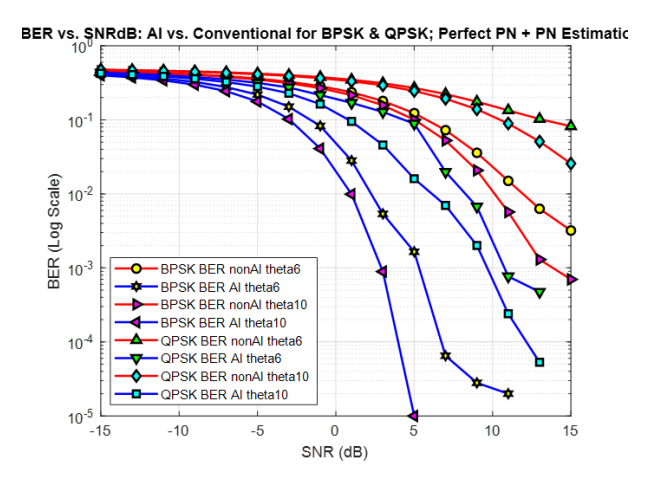


Fig. 4. BER vs SNRdB: AI-based vs. Conventional at Different PN States.

In our investigation across different PN levels, the BPSK MLC DL-assisted DeNMC model demonstrated a more rapid decline in BER compared to the QPSK DeNMC model, particularly as SNR increased. Remarkably, the BPSK model consistently outperformed QPSK, producing a smoother and optimized BER vs. SNR curve. This highlights the superiority of BPSK in THz wireless communication, attributed to its simplicity as a modulation scheme with only two phase states (0 and 180 degrees), in contrast to QPSK's four states (0, 90, 180, and 270 degrees).

Our proposed BPSK exhibited enhanced spectral efficiency, effectively utilizing available bandwidth compared to QPSK. Furthermore, the BPSK MLC DL-assisted DeNMC demonstrated superior robustness, benefitting from its binary nature and fewer phase states, making it less susceptible to phase errors. Consequently, our BPSK results showcased improved performance in the presence of THz impairments, leading to a lower BER. The inherent simplicity of BPSK also contributed to reduced computational complexity in designing the transmitter and receiver components of the THz wireless communication system, underscoring its practical advantages in achieving improved performance and reliability in challenging

THz communication environments. Lastly, Fig. 4 shows that the AI and non-AI curves for both BPSK and QPSK followed the same pattern for all PN states, which demonstrates that our model can effectively work at any phase noise level.

V. CONCLUSION

In this research, a MLC DL assisted DeNMC was developed for a THz wireless communication system. Utilizing supervised learning with a comprehensive dataset spanning a wide SNR range, the MLC DL assisted DeNMC demonstrated superior performance compared to conventional demodulators and decoders. Notably, lower BER was achieved, particularly at low and mid SNRs.

The study delved into the intricate relationship between phase noise, IQ imbalance, compensation techniques, and THz communication system performance. Experimental results highlighted the effectiveness of the proposed DeNMC in mitigating impairments, emphasizing its significance in real-world scenarios with varying SNR conditions that pose challenges to transmission reliability. Leveraging deep learning, the DeNMC showcased enhanced error correction capabilities beyond traditional algorithms, particularly in the presence of phase noise and IQ imbalance.

Furthermore, the application of DNN-based channel decoders represents a pioneering advancement in the realm of error correction for communication systems employing linear block codes. The profound ability of these decoders to grasp intricate mappings between noisy and clean codewords has been demonstrated, showcasing a substantial potential for elevating the error correction performance in such communication systems. The nuanced understanding and adaptive learning capabilities of DNN-based channel decoders empower them to discern complex patterns and dependencies within the encoded data, thus surpassing the conventional methodologies. This transformative potential opens avenues for optimizing the reliability and accuracy of communication systems operating with linear block codes, promising a future where DNN-based decoders become indispensable tools in achieving superior error correction outcomes. The research signifies a crucial step forward in advancing the robustness and efficiency of communication protocols, paving the way for a new era of high-fidelity data transmission across linear block-coded communication channels.

REFERENCES

- M. Giordani, M. Polese, M. Mezzavilla, S. Rangan and M. Zorzi, "Toward 6G Networks: Use Cases and Technologies," in IEEE Communications Magazine, vol. 58, no. 3, pp. 55-61, March 2020, doi: 10.1109/MCOM.001.1900411.
- [2] I. Ahmed, W. Xu, R. Annavajjala and W. -S. Yoo, "Joint Demodulation and Decoding with Multi-Label Classification Using Deep Neural Networks," 2021 International Conference on Artificial Intelligence in Information and Communication (ICAIIC), Jeju Island, Korea (South), 2021, pp. 365-370, doi: 10.1109/ICAIIC51459.2021.9415182.
- [3] E. Nachmani, Y. Be'ery and D. Burshtein, "Learning to decode linear codes using deep learning", 2016 54th Annual Allerton Conference on Communication Control and Computing (Allerton), pp. 341-346, 2016.
- [4] E. Nachmani, E. Marciano, L. Lugosch, W. J. Gross, D. Burshtein and Y. Be'ery, "Deep learning methods for improved decoding of linear codes", IEEE Journal of Selected Topics in Signal Processing, vol. 12, no. 1, pp. 119-131, 2018.

- [5] Y. He, M. Jiang, X. Ling and C. Zhao, "Robust bicm design for the ldpc coded dco-ofdm: A deep learning approach", IEEE Transactions on Communications, vol. 68, no. 2, pp. 713-727, 2020.
- on Communications, vol. 68, no. 2, pp. 713-727, 2020.

 [6] H. He, C. Wen, S. Jin and G. Y. Li, "Deep learning-based channel estimation for beamspace mmwave massive mimo systems", IEEE Wireless Communications Letters, vol. 7, no. 5, pp. 852-855, 2018.
- [7] J. Sun, Y. Zhang, J. Xue and Z. Xu, "Learning to search for mimo detection", IEEE Transactions on Wireless Communications, vol. 19, no. 11, pp. 7571-7584, 2020.
- [8] H. Ye, G. Y. Li and B. Juang, "Power of deep learning for channel estimation and signal detection in OFDM systems", IEEE Wireless Commun. Letters, vol. 7, no. 1, pp. 114-117, Feb 2018.
- [9] Z. Qin, H. Ye, G. Y. Li and B. F. Juang, "Deep learning in physical layer communications", IEEE Wireless Commun, vol. 26, no. 2, pp. 93-99, April 2019.
- [10] S. Akın, M. Penner and J. Peissig, Joint channel estimation and data decoding using sym-based receivers, 2020, [online] Available: https://arxiv.org/abs/2012.02523v1.
- [11] N. Farsad and A. J. Goldsmith, "Detection algorithms for communication systems using deep learning", CoRR, vol. abs/1705.08044, 2017, [online] Available: http://arxiv.org/abs/1705.08044.
- [12] A. S. Mohammad, N. Reddy, F. James and C. Beard, "Demodulation of faded wireless signals using deep convolutional neural networks", 2018 IEEE 8th Annual Computing and Communication Workshop and Conference (CCWC), pp. 969-975, 2018.
- [13] H. Wang, Z. Wu, S. Ma, S. Lu, H. Zhang, G. Ding, et al., "Deep learning for signal demodulation in physical layer wireless communications: Prototype platform open dataset and analytics", IEEE Access, vol. 7, pp. 30 792-30 801, 2019.
- [14] A. C. Vaz, C. G. Nayak and D. Nayak, "Hamming code performance evaluation using artificial neural network decoder", 2019 15th International Conference on Engineering of Modern Electric Systems (EMES), pp. 37-40, 2019.
- [15] H. S. Park, E. -Y. Choi, Y. S. Song, S. Noh and K. Seo, "DNN-based Phase Noise Compensation for Sub-THz Communications," 2020 International Conference on Information and Communication Technology Convergence (ICTC), Jeju, Korea (South), 2020, pp. 866-868, doi: 10.1109/ICTC49870.2020.9289411.
- [16] Y. Jiang, H. Wang, B. Deng, Y. Qin and K. Liu, "A random phase compensation method for terahertz radar," 2016 CIE International Conference on Radar (RADAR), Guangzhou, China, 2016, pp. 1-3, doi: 10.1109/RADAR.2016.8059555.
- [17] Brandonisio, F., Kennedy, M.P. (2014). Modelling and Estimating Phase Noise with Matlab. In: Noise-Shaping All-Digital Phase-Locked Loops. Analog Circuits and Signal Processing. Springer, Cham. https://doi.org/10.1007/978-3-319-03659-5-7.
- [18] N. Chakraborty, M. R. Kadir and M. A. Hossain, "Blind Estimation and Compensation of IQ imbalance in OFDM system," 2013 International Conference on Electrical Information and Communication Technology (EICT), Khulna, Bangladesh, 2014, pp. 1-4, doi: 10.1109/EICT.2014.6777886.
- [19] A. Lomayev, V. Kravtsov, M. Genossar, A. Maltsev and A. Khoryaev, "Method for Phase Noise Impact Compensation in 60 GHz OFDM Receivers," Radioengineering, vol. 29, no. 1, pp. 159-173, April 2020, doi: 10.13164/re.2020.0159.
- [20] I. Goodfellow, Y. Bengio and A. Courville, Deep Learning, MIT Press, 2016, [online] Available: http://www.deeplearningbook.org.
- [21] Min-Ling Zhang and Zhi-Hua Zhou, "Multilabel neural networks with applications to functional genomics and text categorization", IEEE Transactions on Knowledge and Data Engineering, vol. 18, no. 10, pp. 1338-1351, 2006.
- [22] J. Brownlee, Multi-label classification with deep learning, [online] Available: https://machinelearningmastery.com/multi-labelclassificationwith-deep-learning/.
- [23] S. Grunau, D. Block and U. Meier, Multi-label wireless interference identification with convolutional neural networks, 2018.
- [24] I. Ahmed and E. J. Allen, "Deep learning based diversity combining for generic noise and interference", 2020 IEEE 91st Vehicular Technology Conference (VTC2020-Spring), pp. 1-4, 2020.
- [25] Ren, Aifeng et. al., "Terahertz (THz) application in food contamination detection." (2019), 10.1049/SBEW542E.
- [26] M. Abadi et. al., "Tensorflow: Large-scale machine learning on heterogeneous distributed systems." 2016, [online] Available: http://arXiv.org/abs/1603.04467.